

Phase diagram of spin-1 antiferromagnetic Bose-Einstein condensates

David Jacob,¹ Lingxuan Shao,¹ Vincent Corre,¹ Tilman Zibold,¹ Luigi De Sarlo,¹
Emmanuel Mimoun,¹ Jean Dalibard,^{1,2} and Fabrice Gerbier^{1,*}

¹Laboratoire Kastler Brossel, CNRS, ENS, UPMC, 24 rue Lhomond, 75005 Paris

²Collège de France, 11 place Marcelin Berthelot, 75231 Paris, France

(Received 10 September 2012; published 5 December 2012)

We study experimentally the equilibrium phase diagram of a spin-1 Bose-Einstein condensate with antiferromagnetic interactions, in a regime where spin and spatial degrees of freedom are decoupled. For a given total magnetization m_z , we observe for low magnetic fields an “antiferromagnetic” phase where atoms condense in the $m = \pm 1$ Zeeman states, and occupation of the $m = 0$ state is suppressed. Conversely, for large enough magnetic fields, a phase transition to a “broken-axisymmetry” phase takes place: The $m = 0$ component becomes populated and rises sharply above a critical field $B_c(m_z)$. This behavior results from the competition between antiferromagnetic spin-dependent interactions (dominant at low fields) and the quadratic Zeeman energy (dominant at large fields). We compare the measured B_c as well as the global shape of the phase diagram with mean-field theory, and find good quantitative agreement.

DOI: [10.1103/PhysRevA.86.061601](https://doi.org/10.1103/PhysRevA.86.061601)

PACS number(s): 67.85.-d, 03.75.Hh, 05.30.Jp

One of the most active topics in the field of ultracold quantum gases is the study of interacting many-body systems with spin [1–4]. Atoms with arbitrary Zeeman structure can be trapped using far-detuned optical traps. Quantum gases of bosons with spin 1 [3,4], 2 [5,6], or 3 [7] and fermions with spin larger than 1/2 [8,9] have been demonstrated experimentally. This opens a whole class of new experiments with spinful many-body systems, such as coherent spin-mixing dynamics analogous to an internal Josephson effect [5,6,10–14], squeezing among the different spin components [15–17], or the study of sudden quenches across magnetic phase transitions [18,19].

The simplest example is the spin-1 Bose gas. The spin-dependent interaction between two atoms with spins \mathbf{s}_1 and \mathbf{s}_2 can be written as $V_{12} = g_s \mathbf{s}_1 \cdot \mathbf{s}_2$. Depending on the sign of the coupling constant g_s , this interaction leads to either ferromagnetic ($g_s < 0$, the case of atomic ^{87}Rb [10]) or antiferromagnetic ($g_s > 0$, the case of atomic ^{23}Na [20]) behavior. This naturally leads to different equilibrium phases. An additional but essential feature in experiments with gases of alkali-metal atoms is the conservation of the longitudinal magnetization $m_z = n_{+1} - n_{-1}$, which follows from the spin rotational symmetry of V_{12} . Here n_m denotes the relative populations of the Zeeman state labeled by the magnetic quantum number $m = 0, \pm 1$. The only possible spin-changing two-body process is

$$m = 0 + m = 0 \rightarrow m = +1 + m = -1, \quad (1)$$

where two $m = 0$ atoms collide to yield one atom in each state $m = \pm 1$ (or vice-versa), leaving m_z unchanged. In most physical systems, the magnetization would relax by coupling to an external environment. In contrast, quantum gases are almost perfectly isolated and the conservation of magnetization plays a major role [21].

In spite of intense theoretical activity [4], the equilibrium properties of spinor gases remain relatively unexplored experimentally. Most experimental work so far has focused on dynamical properties. For ferromagnetic rubidium condensates,

a recent experimental study concluded that the time needed to reach an equilibrium state, typically several seconds or tens of seconds, could easily exceed the condensate lifetime [22]. For antiferromagnetic ^{23}Na , the stationary regime after damping of spin-mixing oscillations has been studied for relatively high magnetization ($m_z \lesssim 0.5$) [14]. Here also, long equilibration times on the order of 10 s were observed. Both experiments worked with condensates with large atom numbers, well in the Thomas-Fermi regime, where spin domains are expected and observed in transient regimes.

In this Rapid Communication, we present an experimental study of the phase diagram of spin-1 sodium Bose-Einstein condensates with antiferromagnetic interactions. We work with small atomic samples containing a few thousand atoms held in a tightly focused optical trap. In this regime, spin domains are energetically costly, and spatial and spin degrees of freedom are largely decoupled. We prepare the sample well above the condensation temperature with a well-defined longitudinal magnetization and no spin coherence. At the end of the cooling stage, equilibration times of 3 s are used to ensure that thermal equilibrium is reached. We find, in agreement with theoretical predictions, a phase transition from an “antiferromagnetic” phase where only the $m = \pm 1$ Zeeman components are populated to a mixed “broken-axisymmetry” phase where all three Zeeman states can coexist. We determine the phase boundary and the shape of the phase diagram versus applied magnetic field and magnetization by measuring the population of the $m = 0$ state. Our measurements can be explained quantitatively by mean-field theory in the single-mode regime, where the atoms condense in the same spatial wave function irrespective of their internal state.

We work with sodium atoms cooled deeply in the quantum-degenerate regime using an all-optical cooling sequence [23,24]. In order to prepare the sample with a well-defined longitudinal magnetization and no spin coherences, we start from a cold cloud in a crossed optical dipole trap loaded from a magneto-optical trap [24], with a magnetization $m_z \approx 0.6$ resulting from the laser cooling process. To obtain higher degrees of spin polarization, we perform evaporative cooling in the presence of a vertical magnetic field gradient for about 1 s.

*fabrice.gerbier@lkb.ens.fr

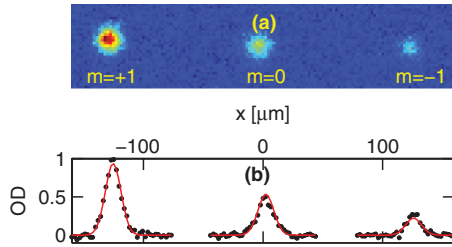


FIG. 1. (Color online) (a) Absorption image of a spin-1 BEC after expansion in a magnetic gradient. (b) Horizontal cuts through the images in (a). The same function (shown by straight lines), only recentered and reweighted, is used to fit the density profile of each Zeeman state. OD indicates the optical density.

Each Zeeman state experiences a slightly different potential depth. Because of the combined action of gravity and the magnetic gradient, evaporative cooling in this configuration favors the Zeeman state with the higher trap depth [25]. This results in partially or almost fully polarized samples with magnetization up to $m_z \approx 0.85$. To obtain lesser degrees of polarization than the initial value $m_z \approx 0.6$, we remove the gradient and apply instead an additional oscillating field resonant at the Larmor frequency. The two procedures together allow us to prepare well-defined magnetizations ranging from 0 to ≈ 0.85 with good reproducibility and keeping the same evaporative cooling ramp in all cases. After spin preparation, we transfer the cloud in the final crossed dipole trap and resume evaporative cooling (see [26] for more details).

After the evaporation ramp, we obtain quasipure spin-1 Bose-Einstein condensates (BECs) containing $N \approx 5000$ atoms in a trap with average frequency $\bar{\omega} \approx 2\pi \times 0.7$ kHz. To ensure that the cloud has reached a steady state, we allow for an additional hold time of 3 s after the evaporation ramp. We have investigated the dynamics of the spin populations as this hold time is varied for several values of magnetization and applied magnetic field. We found that the populations relaxed to steady-state values with a characteristic $(1/e)$ time smaller than 1 s, much smaller than the finite lifetime of our sample, around 10 s.

The populations of the Zeeman states $m = 0, \pm 1$ are analyzed after expansion in a magnetic field gradient producing a Stern-Gerlach force that accelerates atoms in $m = \pm 1$ in opposite directions. After a given expansion time (typically $t \approx 3.5$ ms), we take an absorption picture of the clouds [see Fig. 1(a)], and count the normalized populations n_m of the Zeeman state $m = 0, \pm 1$. Note that the condensate is in a regime intermediate between the ideal gas and the Thomas-Fermi limits (we estimate a chemical potential $\mu \approx 4\hbar\bar{\omega}$ from a numerical solution of the Gross-Pitaevskii equation).

For a Bose-Einstein condensate held in a tight trap as in our experiment, the energetic cost of spin domains is large (comparable to $\hbar\bar{\omega}$ per atom, much larger than the spin-dependent interaction energy). In this limit, it is reasonable to make the single-mode approximation (SMA) for the condensate wave function [27,28], which amounts to considering that all atoms share the same spatial wave function independently of their internal state; the condensate spin remains as a degree of freedom. To support this approximation, we note that absorption images as in Fig. 1(a) do not reveal any spatial structures or spin

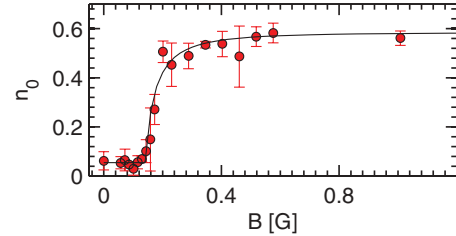


FIG. 2. (Color online) Sample data showing the population n_0 of the $m = 0$ Zeeman state versus applied magnetic field B , for a magnetization $m_z \approx 0.4$. The solid line is a fit to the data using Eq. (5). Vertical error bars show statistical uncertainties on the measured values (one standard deviation).

domains during the 3 s hold time. Furthermore, we compare in Fig. 1(b) the observed distributions with a common mode distribution. This common mode function is extracted from a Gaussian fit to the most populated cloud ($m = +1$ in this example), and then recentered and reweighted to match the populations of the other Zeeman states. We find very good agreement between the three spatial distributions in the whole range of parameters explored, and conclude that the SMA is indeed a good approximation in our case.

Because the longitudinal magnetization $m_z = n_{+1} - n_{-1}$ is conserved, the relevant magnetic energy in an applied magnetic field is the second-order (quadratic) Zeeman shift of magnitude $q = q_B B^2$, with B the applied magnetic field and $q_B \approx 277$ Hz/G². The larger (first-order) linear Zeeman shift has no influence (it can be absorbed in the Lagrange multiplier associated with the fixed magnetization [4]). As other spin-changing mechanisms than collisions are possible, this conservation law is only approximate. For example, it no longer holds when spin flips are induced on purpose by applying oscillating fields as described above, or for systems with magnetic dipole-dipole interactions [7]. In the absence of such applied fields, we find no evidence for violation of this conservation law within our experimental limit of a few percent.

We show in Fig. 2 the measured values of n_0 for a range of applied magnetic fields B and $m_z \approx 0.4$. The population in $m = 0$ is small at low applied fields and rises sharply above a critical value B_c before settling at an asymptotic value. We have repeated these measurements for a wide range of B and m_z , and generically observed this behavior. We show the results in a reconstructed contour plot in Fig. 3(a). The phase diagram shows unambiguously the presence of two different phases which differ in their spin composition, or more precisely are characterized by the absence or presence of condensed atoms in $m = 0$.

We now explain the observed behavior of n_0 in terms of the competition between the spin-dependent interactions and the applied magnetic field (entering quadratically through the second-order Zeeman effect). The mean-field energy functional in the single-mode approximation is given by [4]

$$\frac{E_s}{N} = \frac{U_s}{2} |\mathcal{S}|^2 - qn_0. \quad (2)$$

Here, $\mathcal{S} = \langle \zeta | \hat{S} | \zeta \rangle$ is the expectation value of the spin operator \hat{S} taken in the normalized spinor ζ describing the condensate

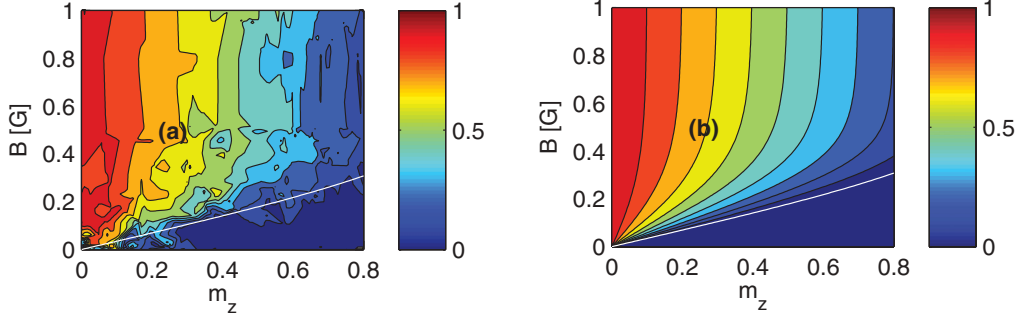


FIG. 3. (Color online) (a) Experimental phase diagram showing the population n_0 of the $m = 0$ Zeeman state versus magnetization m_z and applied magnetic field B . The plot shows a contour interpolation through all data points, with magnetization ranging from 0 to 0.8. The white line is the predicted critical field B_c separating the two phases, deduced from Eq. (4) via $q_c = q_B B_c^2$. (b) Theoretical prediction for n_0 at $T = 0$ K.

spin wave function, and U_s denotes the spin-spin interaction energy (see [26]). For antiferromagnetic interactions ($U_s > 0$), no applied field ($q = 0$) and zero magnetization, the spin-1 BEC realizes a polar, or “spin-nematic,” phase according to mean-field theory [1,2]. The spin wave function ζ belongs to the family of eigenstates of $\hat{S} \cdot \mathbf{n}$ with zero eigenvalue (and zero average spin), with \mathbf{n} a headless vector called the “nematic director” in analogy with the similar order parameter characterizing nematic liquid crystals. When $q = 0$, any direction \mathbf{n} is a possible solution, while any positive q favors occupation of the $m = 0$ state (along z) and pins the nematic director in the z direction.

When m_z is nonzero, there is a competition between the spin-dependent interactions and the quadratic Zeeman energy. The constraint of a fixed magnetization is essential to understand the spin structure of the condensate [29]. The BEC spin wave function can be parametrized generically as [1,2,29]

$$\zeta = \begin{pmatrix} \sqrt{\frac{1}{2}(1-n_0+m_z)}e^{i\phi_{+1}} \\ \sqrt{n_0}e^{i\phi_0} \\ \sqrt{\frac{1}{2}(1-n_0-m_z)}e^{i\phi_{-1}} \end{pmatrix}. \quad (3)$$

We introduced the phases ϕ_m of the components of ζ in the standard basis. The effect of antiferromagnetic spin-dependent interactions ($U_s > 0$) is twofold: First, they lock the relative phase $\phi_{+1} + \phi_{-1} - 2\phi_0$ to π in the minimal-energy state. Second, they favor the coexistence of the $m = \pm 1$ components and disfavor mixing them with the $m = 0$ component [20]. As the quadratic Zeeman energy favors the latter, the competition between the two results in two distinct phases, as observed experimentally.

The equilibrium population n_0 is found by minimizing the mean-field energy functional [29]. For low q and nonzero magnetization m_z , spin-dependent interactions are dominant, and result in a two-component condensate where the Zeeman states $m = \pm 1$ are populated ($n_0 = 0$). Following [3], we will call this phase antiferromagnetic (AF). When $m_z \rightarrow 0$, this gives an “easy-plane” polar phase where the nematic director is confined to the x - y plane. Above a critical value q_c given by

$$q_c = U_s(1 - \sqrt{1 - m_z^2}), \quad (4)$$

n_0 increases continuously from zero, indicating a second-order quantum phase transition. Again following [3], we call this the broken-axisymmetry (BA) phase. For large q , the energy is minimized by increasing n_0 as much as possible given the constraint of a given m_z : The spin populations therefore tend to $n_{+1} = m_z$, $n_0 = 1 - m_z$, and $n_{-1} = 0$ for $m_z > 0$. When $m_z \rightarrow 0$, one recovers the easy-axis polar phase with all atoms in the $m = 0$ state along z . More generally, the BA state with $n_0 \neq 0$ has nonzero longitudinal and transverse magnetization (both vanish when m_z goes to zero), and a nematic director orthogonal to the direction of the magnetization vector [30].

We measured the critical line separating the AF and BA phases using the following procedure. We bin the data according to the measured magnetization, in bins of width 0.1 around an average magnetization from $m_z \approx 0$ to $m_z \approx 0.8$, with residual fluctuations around $\delta m_z \approx 0.02$. Each data set with given magnetization is fitted with a function of the form

$$n_0 = \begin{cases} A_0, & q < q_c, \\ A_0 + A_1 \frac{q - q_c}{q - q_c + \Delta q}, & q \geq q_c. \end{cases} \quad (5)$$

This form ensures the existence of a sharp boundary determined by q_c , a constant background value for low q , and a well-defined asymptotic value for large q , and reproduces the observed data fairly well, as shown in Fig. 2 for a specific example with $m_z \approx 0.4$. At low fields, n_0 is not strictly zero but takes values of a few percent, which can be explained by the presence of a small noncondensed fraction ($f' \approx 2\%$ – 3% per component). As such small populations are near our detection limit ($\sim 3\%$ for the fractional populations, limited by the optical shot noise associated with the imaging process), we do not attempt to determine them and consider in the following that the condensate is essentially at zero temperature. At high fields, n_0 is very close to the expected value $1 - m_z$ [see Fig. 4(a)], again within a few percent.

We show in Fig. 4(b) the measured boundary $B_c = \sqrt{q_c/q_B}$ between the two phases, which we find in good agreement with the prediction of Eq. (4) in the whole range investigated. The comparison is made with the value $U_s/h \approx 65.6$ Hz, obtained from a numerical solution of the Gross-Pitaevskii equation using the scattering lengths given in [31] and the measured trapping parameters and average atom number, and thus does

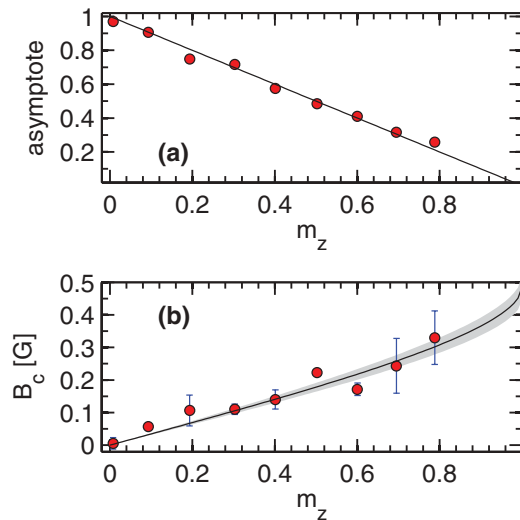


FIG. 4. (Color online) (a) Asymptotic value of n_0 for large q [determined from $A_0 + A_1$ in Eq. (5)]. The solid line shows the value $1 - m_z$ expected at zero temperature. (b) Measured critical field B_c versus magnetization. The solid line shows the values expected from Eq. (4) and $q_c = q_B B_c^2$, using $U_s/h \approx 65.6$ Hz. The gray area shows the 15% uncertainty on the theoretical value of B_c , dominated by the 15% uncertainty on the spin-dependent scattering length a_s . For both plots, vertical error bars show statistical uncertainties on the measured values (one standard deviation).

not require any fitting parameter. Our results are in line with previous measurements in [14], which were restricted to the range $m_z > 0.5$ and $B > 0.2$ G and performed with much larger samples well in the Thomas-Fermi regime. Here, we are able to characterize this transition down to zero magnetization and zero applied field, in a system where spin domains (as

observed in [14] during the relaxation towards equilibrium) are not expected to form.

Mean-field theory also quantitatively describes our data above the critical line. We compare the calculated n_0 directly to the data in Figs. 3(a) and 3(b). There are no adjustable parameters in this comparison, since the parameters used in the theory are either measured or computed independently. The shape and magnitude of the calculated phase diagram matches the measured one within 10% at worst, except very close to the origin $B \approx 0$ and $m_z \approx 0$. In this corner of the phase diagram, we observe larger deviations from the mean-field prediction and correspondingly higher fluctuations in n_0 . We will present a detailed study of these findings in another presentation.

In conclusion, we have explored experimentally the phase diagram of spin-1 BECs with antiferromagnetic interactions. Two phases are found, reflecting the competition between the spin-dependent interactions and the quadratic Zeeman energy. The measurements are in quantitative agreement with mean-field theory, which quantitatively predicts the phase boundary but also the observed spin populations above the transition. In this paper, the population of noncondensed atoms was small (a few percent, below our detection level). Although interesting effects beyond the mean field are predicted at very low temperatures [32], they would require much better sensitivity and lower temperatures to be addressed. On the other hand, at higher temperatures the thermodynamics should differ substantially from the scalar case [7,33]. Both paths provide interesting directions for future work.

We thank B. Laburthe-Tolra, O. Gorceix, and P. Lett for useful discussions. This work was supported by IFRAF, by Ville de Paris (Emergences Project), and by DARPA (OLE Project).

-
- [1] T.-L. Ho, *Phys. Rev. Lett.* **81**, 742 (1998).
 [2] T. Ohmi and T. Machida, *J. Phys. Soc. Jpn.* **67**, 1822 (1998).
 [3] M. Ueda and Y. Kawaguchi, [arXiv:1001.2072v2](https://arxiv.org/abs/1001.2072v2).
 [4] D. M. Stamper-Kurn and M. Ueda, [arXiv:1205.1888](https://arxiv.org/abs/1205.1888).
 [5] H. Schmaljohann, M. Erhard, J. Kronjäger, M. Kottke, S. van Staa, L. Cacciapuoti, J. J. Arlt, K. Bongs, and K. Sengstock, *Phys. Rev. Lett.* **92**, 040402 (2004).
 [6] T. Kuwamoto, K. Araki, T. Eno, and T. Hirano, *Phys. Rev. A* **69**, 063604 (2004).
 [7] B. Pasquiou, E. Maréchal, L. Vernac, O. Gorceix, and B. Laburthe-Tolra, *Phys. Rev. Lett.* **108**, 045307 (2012).
 [8] S. Taie, Y. Takasu, S. Sugawa, R. Yamazaki, T. Tsujimoto, R. Murakami, and Y. Takahashi, *Phys. Rev. Lett.* **105**, 190401 (2010).
 [9] J. S. Krauser, J. Heinze, N. Fläschner, S. Götze, C. Becker, and K. Sengstock, [arXiv:1203.0948v1](https://arxiv.org/abs/1203.0948v1).
 [10] M.-S. Chang, C. D. Hamley, M. D. Barrett, J. A. Sauer, K. M. Fortier, W. Zhang, L. You, and M. S. Chapman, *Phys. Rev. Lett.* **92**, 140403 (2004).
 [11] M.-S. Chang, Q. Qin, W. Zhang, L. You, and M. S. Chapman, *Nat. Phys.* **1**, 111 (2005).
 [12] J. Kronjäger, C. Becker, M. Brinkmann, R. Walser, P. Navez, K. Bongs, and K. Sengstock, *Phys. Rev. A* **72**, 063619 (2005).
 [13] A. T. Black, E. Gomez, L. D. Turner, S. Jung, and P. D. Lett, *Phys. Rev. Lett.* **99**, 070403 (2007).
 [14] Y. Liu, S. Jung, S. E. Maxwell, L. D. Turner, E. Tiesinga, and P. D. Lett, *Phys. Rev. Lett.* **102**, 125301 (2009).
 [15] B. Lcke, M. Scherer, J. Kruse, L. Pezz, F. Deuretzbacher, P. Hyllus, O. Topic, J. Peise, W. Ertmer, J. Arlt *et al.*, *Science* **334**, 773 (2011).
 [16] C. Gross, H. Strobel, E. Nicklas, T. Zibold, N. Bar-Gill, G. Kurizki, and M. K. Oberthaler, *Nature (London)* **480**, 219 (2011).
 [17] C. D. Hamley, C. S. Gerving, T. M. Hoang, E. M. Bookjans, and M. S. Chapman, *Nat. Phys.* **8**, 305 (2012).
 [18] L. E. Sadler, J. M. Higbie, S. R. Leslie, M. Vengalattore, and D. M. Stamper-Kurn, *Nature (London)* **443**, 312 (2006).
 [19] E. M. Bookjans, A. Vinit, and C. Raman, *Phys. Rev. Lett.* **107**, 195306 (2011).
 [20] J. Stenger, S. Inouye, D. Stamper-Kurn, H.-J. Miesner, A. Chikkatur, and W. Ketterle, *Nature (London)* **396**, 345 (1998).

- [21] This statement holds when magnetic dipole-dipole interactions are negligible, which is the case for alkali atoms. For some atomic species with large magnetic moments, such as Chromium [7], dipolar relaxation can be dominant.
- [22] J. Guzman, G.-B. Jo, A. N. Wenz, K. W. Murch, C. K. Thomas, and D. M. Stamper-Kurn, *Phys. Rev. A* **84**, 063625 (2011).
- [23] E. Mimoun, L. De Sarlo, D. Jacob, J. Dalibard, and F. Gerbier, *Phys. Rev. A* **81**, 023631 (2010).
- [24] D. Jacob, E. Mimoun, L. D. Sarlo, M. Weitz, J. Dalibard, and F. Gerbier, *New J. Phys.* **13**, 065022 (2011).
- [25] A. Couvert, M. Jeppesen, T. Kawalec, G. Reinaudi, R. Mathevet, and D. Gury-Odelin, *Europhys. Lett.* **85**, 19901 (2009).
- [26] See Supplemental Material at <http://link.aps.org/supplemental/10.1103/PhysRevA.86.061601> for more details.
- [27] C. K. Law, H. Pu, and N. P. Bigelow, *Phys. Rev. Lett.* **81**, 5257 (1998).
- [28] S. Yi, O. E. Müstecaplıoğlu, C. P. Sun, and L. You, *Phys. Rev. A* **66**, 011601 (2002).
- [29] W. Zhang, S. Yi, and L. You, *New J. Phys.* **5**, 77 (2003).
- [30] F. Zhou, M. Snoek, J. Wiemer, and I. Affleck, *Phys. Rev. B* **70**, 184434 (2004).
- [31] S. Knoop, T. Schuster, R. Scelle, A. Trautmann, J. Appmeier, M. K. Oberthaler, E. Tiesinga, and E. Tiemann, *Phys. Rev. A* **83**, 042704 (2011).
- [32] N. T. Phuc, Y. Kawaguchi, and M. Ueda, *Phys. Rev. A* **84**, 043645 (2011).
- [33] W. Zhang, S. Yi, and L. You, *Phys. Rev. A* **70**, 043611 (2004).